Theoretical study into a novel design of Oscillating Water Column with high broadbanded efficiency

Sasha Parry-Barnard[1] and Richard Porter[2]

[1]Mathematics Department, University College London, 25 Gordon Street, London WC1H 0AY, UK

[2]School of Mathematics, Fry Building, Woodland Road, Bristol, BS8 1UG, UK

Corresponding author: Sasha Parry-Barnard, sasha.barnard.25@ucl.ac.uk

(Received xx; revised xx; accepted xx)

This paper considers the theoretical operation of a novel wall-mounted oscillating water column wave energy device designed to be resonant over a broad range of frequencies. A curved duct with a submerged opening in a vertical wall is partitioned into a number of separate narrow channels of uniform width using thin annular baffles. Each channel connects the submerged opening to its own internal free surface whose rise and fall drives the air enclosed above through a Wells-type turbine through which energy is harvested. The different channel lengths within the duct encourages, when subjected to forcing from incident waves, resonance across a range of frequencies. The two-dimensional problem described in this work is analysed using classical linearised water wave theory and the geometric complexity of the partitioned duct is simplified by homogenisation. This allows the solution to the water wave problem to be reduced to a scalar integral equation whose solution is approximated using a standard numerical method. It is shown that it is possible, even with the most basic choice of turbine power take-off strategies, to achieve efficiencies close to 100% across much of the range of frequencies defined by the resonance associated with the longest and shortest channels of the device. Viscous damping within the channels is shown to have a negligible effect for practical configurations.

Key words: Surface gravity waves, Wave-structure interactions, Coastal engineering

1. Introduction

The Oscillating Water Column (OWC) concept (see Heath (2012), Falcão & Henriques (2016), for example) is, to date, arguably the most commercially successful device for converting ocean wave energy into electricity. Originally devised by Yoshio Masuda in the 1940s as a means of powering floating navigation buoys (see Masuda (1985)), a number of modestly-sized plants have been installed in a variety of settings and operated with some success, supplying energy to national electrical grids. For a recent review, see Gayathri *et al.* (2024).

OWCs operate by isolating an internal air chamber from the open ocean via a surface-piercing lip with an opening below the water line. The rise and fall of incoming waves forces the enclosed air above the internal free surface back and forth through an air turbine whose role is to generate electrical energy. A self-rectifying turbine, such as a Wells turbine (described in Falcão & Henriques (2016)), is typically used; it is designed to spin in the same direction regardless of the direction of the air flow. The success of the OWC lies in its simplicity: the only moving part is the air turbine, located above the water line. Being typically mounted at the shoreline mitigates the expense and difficulty of mooring, power transmission and maintenance operations associated with offshore wave energy devices. On the other hand, shore-mounted OWCs such as Kvaerner in Norway (see Falnes (1993)), the pilot plants of PICO in the Azores (see Falcão *et al.* (2020)) and LIMPET on the Scottish Island of Islay (see Boake *et al.* (2002)) are considered difficult to build with site-specific constraints and a significant environmental impact. Additionally, the nearshore wave energy resource is not as high as far offshore whilst being more vulnerable to violent wave breaking events. Projects in Japan, India, China, Italy and Spain have involved installing OWC units into sea walls to serve a dual purpose of coastal/harbour protection and energy generation. To date, the largest and most successful of these is the Mutriku Wave Power Plant on the northern coast of Spain. It comprises 16 OWCs set side-by-side in a harbour wall, rated at 296kW, and in operation since 2011. It has since supplied over 3GWh to the grid (see Lopez-Mendia *et al.* (2025)).

It was the during the initial surge in interest in wave energy in the response to the oil crisis of 1973 that the theoretical basis for the operation of wave energy converters, including OWCs, was established (for an overview see Evans (1981)). Early, but instructive, work on the OWC concept by Evans (1978) applied rigid-body theory to a simple OWC model. By modelling the internal free surface as a weightless piston, it was demonstrated that the resonant motion of the fluid within the internal chamber can be excited at certain incident wave frequencies dependent on the depth of submergence of the duct. Shortly afterwards, Falcão & Sarmento (1980) correctly accounted for the internal free surface using a theory based on oscillating pressure variations within the air chamber of the OWC device. This led to the general theoretical framework for multiple interacting OWCs described by Evans (1982). Some years later Evans & Porter (1995), revisiting a problem initially considered by Smith (1983), showed how a simple two-dimensional model of a shore-mounted OWC could extract 100% of the incoming wave energy at an isolated resonant frequency dependent on the size and shape of the submerged rectangular chamber. In Evans & Porter (1995) only curves showing the maximum theoretical efficiency were shown whilst the effect of air compressibility was overlooked. Porter (2025) has produced a recent update of that paper addressing both these issues, showing that 100% efficiency can still be achieved at a specific frequency associated with resonance and for a carefully-tuned power control. Results highlight the effect that both non-optimally tuned power take-off and air compressibility have on efficiency showing how efficiency can fall well below the theoretical maximum presented in the work of Evans & Porter (1995).

The modelling of OWCs has advanced over the last 30 years and many theoretical studies have been made of more complex OWC geometries in more realistic three-dimensional settings including arrays of devices. See, for example, Martin-Rivas & Mei (2009), Zheng *et al.* (2019) and references therein. In this paper we return to the simpler two-dimensional setting in order to assess how a shift in fundamental OWC design affects its performance. A submerged opening is connected to an internal free surface via an annular duct which is divided into N (we suppose many) separate narrow annular channels with thin, rigid, curved baffles. The air enclosed above each narrow channel is connected to the atmosphere via its own Wells turbine. The idea of the design is to broaden the device response. Since there

are N channels of different lengths, the proposed device possesses resonances at N closely-spaced frequencies, the largest/smallest of which are associated with the shortest/longest channels within the array.

The idea of engineering multiple resonant frequencies within a single device is not new. For example, the Belfast OWC concept of the 1970s (see Whittaker *et al.* (1985)) had two chambers tuned to two different frequencies housed within a circular device. The Kvaerner device described by Falnes (1993) was unique in that it was built into a natural harbour to couple harbour resonance with device resonance. Closely related to the current proposal, Wilks *et al.* (2022) considered a theoretical two-dimensional concept comprised of multiple vertical channels of gradually increasing submerged depth separated by thin vertical baffles. The oscillations of the fluid powered rigid pistons placed on the surface of each channel and it was shown that efficiency close to 100% across a broad range of frequencies could be achieved. The design of Wilks *et al.* (2022) was guided as much by the principle of graded arrays and so-called rainbow reflection (the slowing of effective wave speed) as it was by multiple resonance. Very recently, Hu *et al.* (2025) have considered the modification of the Wilks *et al.* (2022) where rigid pistons are replaced by OWC chambers. In their work, 5 vertical channels of increasing immersed depth are considered using computational fluid dynamics simulations which include turbulent effects and air compressibility, whilst the incoming waves propagate from a model energy density spectrum. Despite turbulent losses caused by flow separation around the sharp edges of the thin vertical barriers, the authors report a broadband efficiency of more than 50% over the range of resonant frequencies.

The OWC device described in this paper is really a closely-packed system of N coupled OWC devices, and so formally the general theory of Evans (1982) applies. However, a different approach is taken here, one which has proved successful in other application areas. The geometric complexity of the baffle-partitioned duct is replaced with an effective medium using asymptotic homogenisation. This process is described in Section 2 of the paper in the midst of the formulation of the problem and its solution. It formally applies for $N \gg 1$, but in other problems has been shown to provide a good approximation to the geometrically exact solution, provided the length to width ratio of the channels is sufficiently large (roughly a factor of 10). See, for example, Liang *et al.* (2024) who considered plane wave scattering parallel arrays of thin closely-spaced plates. In Section 2 it is shown how this simplification allows the problem to be reduced to a single scalar integral equation solution. This is approximated numerically, in Section 4 of the paper, using Galerkin's method. Two expressions for the efficiency of power capture are derived in Section 3, one based on power capture at the device and one based on a far-field energy flux calculation. These lead to independent numerical methods for computing the device efficiency which is useful for validating the implementation of the numerical method. In Section 5 we describe the simple changes needed to incorporate the damping effect of viscous boundary layers due the oscillating fluid flow in the multiple narrow channels of the duct. The results are presented in Section 6 where we consider the effects of air compressibility and viscous damping. A summary of the paper with an outlook on the prospects for the design is given in Section 7.

2. Problem specification and solution

Two-dimensional Cartesian coordinates, (x, z), are used, $z = 0$ corresponding to the rest position of the fluid surface and z directed vertically downwards. In $x < 0$ the fluid depth is taken to be a constant, h. At $x = 0$ a vertical wall extends upwards from $z = h$ to $z = b$ and from $z = a$ through the surface. The gap in the wall $a < z < b$ connects the fluid in $x < 0$ to an internal fluid surface in $a < x < b$ via a curved annular duct in $x > 0$. Its inner

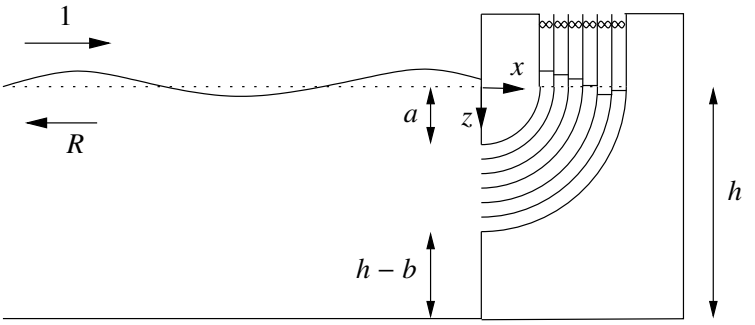

Figure 1. Definition sketch of the OWC device with N curved fluid filled channels with internal free surfaces above which air is pumped from an enclosed chamber through air turbines, indicated by bow ties.

and outer walls are described in polars coordinates, (r, θ) with $x = r\sin\theta$, $z = r\cos\theta$, by $r = a$ and $r = b$ for $0 \le \theta \le \pi/2$. The duct is divided into N curved channels of uniform width by $N - 1$ thin internal curved baffles along $r = r_j$, $1 \le j \le N - 1$ $0 \le \theta \le \pi/2$ where $r_j = a + j\Delta$ for $0 \le j \le N$. Thus $\Delta = (b - a)/N$ is the uniform width of each fluid channel and we suppose that N is large enough that Δ/a is suitably small. This quantity defines the largest aspect ratio of width to length within the array of N fluid channels and its smallness is needed for the method of solution we propose.

It is supposed that above the internal free surface of each of the N partitioned channels lies an air chamber, which is isolated from the other N channels and connected to the external atmosphere by a duct containing its own self-rectifying Wells air turbine. Thus, when the fluid is set into motion, the rise and fall of the internal fluid surface within each channel drives the air back and forth through the turbine.

The water is assumed to be incompressible, inviscid (although viscous effects are considered later in the paper) and has density ρ; its motion is assumed to be of small amplitude and irrotational. This allows us describe the fluid velocity as the gradient of a velocity potential $\Phi(x, z, t)$ which we express as

$$\Phi(x, z, t) = \Re\{-(\mathrm{i}gA/\omega)\phi(x, z)\mathrm{e}^{-\mathrm{i}\omega t}\} \tag{2.1}$$

where $A \in \mathbb{C}$ is the incident wave amplitude (encoding a modulus and phase) and g is acceleration due to gravity. We have anticipated the linearity of the governing equations that follow implying that a monochromatic incident wave of angular frequency ω drives a response of the same frequency thereby allowing us to remove a time-harmonic factor from the motion; $\phi(x, z)$ is consequently a complex-valued velocity potential satisfying

$$\nabla^2\phi = 0 \tag{2.2}$$

everywhere in the fluid. The surface elevation (measured upwards from $z = 0$) is represented by $\zeta(x, t) = \Re\{A\eta(x)\mathrm{e}^{-\mathrm{i}\omega t}\}$ such that the linearised kinematic condition can be written as

$$K\eta(x) = -\phi_z(x, 0), \qquad (K = \omega^2/g) \tag{2.3}$$

on all free surfaces: both in $x < 0$, and in each of the channels across $a < x < b$. The pressure is defined as $P(x, z, t) = P_a + \Re\{A\rho g p(x, z)\mathrm{e}^{-\mathrm{i}\omega t}\}$ where P_a is the atmospheric pressure. Use of the linearised Bernoulli equation

$$P(x, z, t) = P_a - \rho\Phi_t + \rho g z \tag{2.4}$$

on the free surface $z = -\zeta(x,t)$, gives

$$\phi(x,0) - \eta(x) = 0, \qquad x < 0 \tag{2.5}$$

and on each internal free surface $r_{j-1} < x < r_j$ $(j = 1,\dots,N)$ we have

$$p_j = \phi(x,0) - \eta(x) \tag{2.6}$$

where $p = p_j$ represents the oscillating air pressure in the chamber above the jth channel. Combining (2.3) with (2.4) and (2.5) results in

$$\phi_z(x,0) + K\phi(x,0) = \begin{cases} 0, & x < 0 \\ Kp_j, & r_{j-1} < x < r_j. \end{cases} \tag{2.7}$$

The oscillating pressure drives a flow through the air turbine connected to the jth channel which is assumed to obey a standard semi-empirical law (see Sarmento & Falcão (1985), Martin-Rivas & Mei (2009)) relating pressure to the volume flux (per unit length) of fluid, $Q(t)$, across the mean free surface via

$$Q(t) = \lambda_1(P - P_a) + \lambda_2 \frac{\mathrm{d}P}{\mathrm{d}t}. \tag{2.8}$$

When applied in channel j (2.8) reduces to

$$q_j = \mathrm{i}\Lambda_j p_j \tag{2.9}$$

where

$$q_j = -\int_{r_{j-1}}^{r_j} \phi_z(x,0)\,\mathrm{d}x \tag{2.10}$$

represents the volume flux (per unit length) of fluid crossing $z = 0$. In (2.9)

$$\Lambda_j = \rho\omega\lambda_{1,j} - \mathrm{i}\rho\omega^2\lambda_{2,j}. \tag{2.11}$$

The law (2.8), applied to channel j, accounts for the compressibility of air (Sarmento & Falcão (1985), Martin-Rivas & Mei (2009)) with

$$\lambda_{2,j} = \frac{V_j}{\rho_a c_a^2} \tag{2.12}$$

where ρ_a is air density, V_j is the volume of air (per unit length) in the jth chamber (with respect to the rest position of the fluid) and c_a is the speed of sound in air. The parameter $\lambda_{1,j}$ can be written in terms of the control and design parameters of a Wells turbine, but we imagine this is a free power control parameter.

No flow conditions apply on all fixed submerged boundaries in the flow and this is expressed as

$$\partial\phi/\partial n = 0, \tag{2.13}$$

representing the vanishing of the normal derivative of ϕ.

Finally, we need to impose a condition in the far field and write

$$\phi(x,z) = (\mathrm{e}^{\mathrm{i}kx} + R\mathrm{e}^{-\mathrm{i}kx})\psi_0(z), \qquad \text{as } x \to -\infty \tag{2.14}$$

where $R \in \mathbb{C}$ is the reflection coefficient and

$$\psi_0(z) = \cosh k(h-z)/\cosh kh \tag{2.15}$$

is the depth dependence associated with propagating waves of wavenumber k, found from separating variables: k is defined to be the positive real root of

$$K = k\tanh kh. \tag{2.16}$$

The standard method of solution for solving the problem of N independent oscillating pressure distributions is to decompose the problem into $N+1$ potentials: the scattering of incident waves in the absence of pressure distributions plus N radiation potentials defined by a prescribed isolated forcing in each of the N channels in the absence of incoming waves. The individual solutions are then coupled via the turbine law connecting volume fluxes and pressures in each of the N channels. The general theory can be found in Evans (1982). However, each problem is complicated and the complete solution is expressed in terms of $N \times N$ matrices. The advantage of this approach it that it does furnish an explicit condition maximising efficiency, but only by supposing that there is complex-valued control coupling each turbine to every other one, which is not practical.

We take a different approach, the first step of which combines the turbine law (2.9), (2.10) with the surface condition (2.7) to eliminate p_j resulting in

$$\phi_z(x,0) + K\phi(x,0) = \mathrm{i}\frac{K}{\Lambda_j}\int_{r_{j-1}}^{r_j} \phi_z(x,0)\,\mathrm{d}x, \qquad r_{j-1} < x < r_j \tag{2.17}$$

$(j = 1, \ldots, N)$.

2.1. *Homogenisation in $x > 0$*

Next, we aim to simplify the complexity of the duct containing the baffles by approximating the problem using homogenisation methods. The basis of this approximation is $\epsilon = \Delta/r_0 \ll 1$ (where $r_0 = a$) implying that the width of the channels is small compared to their length. First we non-dimensionalise the governing Laplace equation (2.2) in the duct by writing $r = r_0\hat{r}$, $\phi(r,\theta) = \hat{\phi}(\hat{r},\theta)$ so that we have

$$\left(\frac{\partial^2}{\partial\hat{r}^2} + \frac{1}{\hat{r}}\frac{\partial}{\partial\hat{r}} + \frac{1}{\hat{r}^2}\frac{\partial}{\partial\theta^2}\right)\hat{\phi}(\hat{r},\theta) = 0, \qquad \hat{r}_{j-1} < \hat{r} < \hat{r}_j,\ 0 < \theta < \tfrac{1}{2}\pi \tag{2.18}$$

for $j = 1, \ldots, N$ where $\hat{r}_j = r_j/r_0$, noting that the condition (2.13) applied to the channel walls is expressed as

$$\frac{\partial\hat{\phi}}{\partial\hat{r}} = 0, \qquad \hat{r} = \hat{r}_j,\ 0 < \theta < \tfrac{1}{2}\pi. \tag{2.19}$$

Next we make a multiple-scales approximation in which $R = \hat{r}/\epsilon$ where $\epsilon = \hat{r}_j - \hat{r}_{j-1} \ll 1$ is the dimensionless distance between adjacent baffles is defined as the fast (channel) scale and we write

$$\hat{\phi}(\hat{r},\theta) = \hat{\phi}_0(\hat{r},R,\theta) + \epsilon\hat{\phi}_1(\hat{r},R,\theta) + \epsilon^2\hat{\phi}_2(\hat{r},R,\theta) + \ldots. \tag{2.20}$$

Consequently (2.18) is to be written as

$$\left(\left(\frac{\partial}{\partial\hat{r}} + \frac{1}{\epsilon}\frac{\partial}{\partial R}\right)^2 + \frac{1}{\hat{r}}\left(\frac{\partial}{\partial\hat{r}} + \frac{1}{\epsilon}\frac{\partial}{\partial R}\right) + \frac{1}{\hat{r}^2}\frac{\partial^2}{\partial\theta^2}\right)\left(\hat{\phi}_0(\hat{r},R,\theta) + \epsilon\hat{\phi}_1(\hat{r},R,\theta) + \ldots\right) = 0,$$
$$0 < R < 1,\ 0 < \theta < \tfrac{1}{2}\pi \tag{2.21}$$

whilst (2.19) becomes

$$\left(\frac{\partial}{\partial\hat{r}} + \frac{1}{\epsilon}\frac{\partial}{\partial R}\right)\left(\hat{\phi}_0(\hat{r},R,\theta) + \epsilon\hat{\phi}_1(\hat{r},R,\theta) + \ldots\right) = 0, \qquad R = 0, 1,\ 0 < \theta < \tfrac{1}{2}\pi. \tag{2.22}$$

From (2.21), (2.22) the $O(1/\epsilon^2)$ problem for $\hat{\phi}_0$ is defined by

$$\frac{\partial^2\hat{\phi}_0}{\partial R^2} = 0, \qquad 0 < R < 1 \tag{2.23}$$

160 with $\partial_R \hat{\phi}_0 = 0$ on $R = 0, 1$. The clearly integrates to give $\hat{\phi}_0 \equiv \hat{\phi}_0(\hat{r}, \theta)$ (i.e. independent
161 of R, the channel scale).

For the problem at $O(1/\epsilon)$ (2.21), (2.22) give

$$\frac{\partial^2 \hat{\phi}_1}{\partial R^2} = 0, \quad 0 < R < 1, \qquad \text{with} \qquad \frac{\partial \hat{\phi}_1}{\partial R} = -\frac{\partial \hat{\phi}_0}{\partial \hat{r}}, \quad \text{on } R = 0, 1 \tag{2.24}$$

and so

$$\hat{\phi}_1(\hat{r}, R, \theta) = -R\frac{\partial \hat{\phi}_0}{\partial \hat{r}} + \chi_1(\hat{r}, \theta) \tag{2.25}$$

where χ_1 is an arbitrary function. From (2.21) the governing equation at $O(1)$ turns out to be, after simplifying using (2.25),

$$\frac{\partial^2 \hat{\phi}_2}{\partial R^2} - \frac{\partial^2 \hat{\phi}_0}{\partial \hat{r}^2} + \frac{1}{\hat{r}^2}\frac{\partial^2 \hat{\phi}_0}{\partial \theta^2} = 0, \qquad 0 < R < 1 \tag{2.26}$$

and the associated boundary conditions are

$$\frac{\partial \hat{\phi}_2}{\partial R} = R\frac{\partial^2 \hat{\phi}_0}{\partial \hat{r}^2} - \frac{\partial \chi_1}{\partial \hat{r}}, \qquad R = 0, 1. \tag{2.27}$$

Integrating (2.26) over $0 < R < 1$ and using (2.27) results in the leading order governing equation for $\hat{\phi}_0$, namely

$$\frac{\partial^2 \hat{\phi}_0}{\partial \theta^2} = 0. \tag{2.28}$$

This is what we might have expected as it implies that the leading order flow is parallel to the channel walls (plug flow); (2.28) integrates to

$$\hat{\phi}_0(\hat{r}, \theta) = B(r_0\hat{r})\theta + C(r_0\hat{r}) \tag{2.29}$$

where B, C are arbitrary functions of the macroscale variable, r. Meanwhile on the boundary $z = 0$, equivalent to $\theta = \frac{1}{2}\pi$, the transformation applied to (2.17) gives

$$\left(Kr_0 - \frac{1}{\hat{r}}\frac{\partial}{\partial \theta}\right)\left(\hat{\phi}_0(\hat{r}, \tfrac{1}{2}\pi) + \ldots\right) = -\mathrm{i}\frac{K\Delta}{\Lambda_j}\int_0^1 \frac{1}{\hat{r}}\frac{\partial}{\partial \theta}\left(\hat{\phi}_0(\hat{r}, \tfrac{1}{2}\pi) + \ldots\right) \mathrm{d}R \tag{2.30}$$

and we write $\Lambda_j = K\Delta\tilde{\Lambda}(r_0\hat{r})$ since it does not depend on R. Consequently

$$\tilde{\Lambda}(r) = \frac{\tilde{\lambda}_1(r)}{\sqrt{K(b-a)}} - \mathrm{i}\tilde{\lambda}_2(r) \tag{2.31}$$

is a dimensionless parameter implying, from (2.11), (2.12), that

$$\tilde{\lambda}_2(r) = \rho g H(r)/\rho_a c_a^2 \tag{2.32}$$

where $H(r)$ measures the height the air chamber as a function of position. Additionally

$$\tilde{\lambda}_1(r) = \frac{\rho\sqrt{g(b-a)}}{\Delta}\lambda_1(r), \tag{2.33}$$

162 like $\tilde{\lambda}_2(r)$, is frequency-independent and related to the geometry and mechanics of the
163 turbine: we regard this as a free parameter, dependent on position r, which controls the
164 damping.

At leading order (2.30) is therefore

$$\left(1-\frac{\mathrm{i}}{\tilde{\Lambda}(r_0\hat{r})}\right)\frac{\partial\hat{\phi}_0}{\partial\theta}(\hat{r},\tfrac{1}{2}\pi)=Kr_0\hat{r}\hat{\phi}_0(\hat{r},\tfrac{1}{2}\pi). \tag{2.34}$$

Now $\phi(r,\theta)=\hat{\phi}(\hat{r},\theta)\approx\hat{\phi}_0(\hat{r},\theta)$ to leading order. So from (2.29) we have

$$\phi(r,\theta)=B(r)\theta+C(r), \qquad \text{for } 0<\theta<\tfrac{1}{2}\pi,\ a<r<b \tag{2.35}$$

where

$$\left(1-\frac{\mathrm{i}}{\tilde{\Lambda}(r)}\right)\frac{\partial\phi}{\partial\theta}=Kr\phi, \qquad \text{on } \theta=\tfrac{1}{2}\pi,\ a<r<b. \tag{2.36}$$

It is useful to define a function $U(r)$ which represents the horizontal fluid velocity along $x=0$, the vertical opening of the duct, so that

$$\frac{1}{r}\frac{\partial\phi}{\partial\theta}\bigg|_{\theta=0}=U(r), \qquad a<r<b. \tag{2.37}$$

It follows that $B(r)=rU(r)$ and then using (2.36) we have

$$\left(1-\frac{\mathrm{i}}{\tilde{\Lambda}(r)}\right)U(r)=K\left(\tfrac{1}{2}\pi rU(r)+C(r)\right) \tag{2.38}$$

which defines $C(r)$ and so, finally,

$$\phi(r,\theta)=rU(r)(\theta-\tfrac{1}{2}\pi)+K^{-1}(1-\mathrm{i}/\tilde{\Lambda}(r))U(r) \tag{2.39}$$

represents the general solution in $x>0$ in terms of a single unknown function, $U(r)$.

2.2. *Solution in $x<0$ and matching*

In $x<0$ we can write the general solution, satisfying (2.2), (2.7) and (2.13) on $z=h$, using separation of variables (see Linton & McIver (2001)), as

$$\phi(x,z)=(\mathrm{e}^{\mathrm{i}kx}+R\mathrm{e}^{-\mathrm{i}kx})\psi_0(z)+\sum_{n=1}^{\infty}\frac{\psi_n(z)\mathrm{e}^{k_nx}}{N_nk_nh}\int_a^b U(z')\psi_n(z')\,\mathrm{d}z' \tag{2.40}$$

where, for $n\geq1$,

$$\psi_n(z)=\cos k_n(h-z)/\cos k_nh \tag{2.41}$$

and k_n are the positive real roots of $K=-k_n\tan k_nh$, ordered in increasing size. The functions $\psi_n(z)$ are orthogonal, satisfying

$$\frac{1}{h}\int_0^h\psi_m(z)\psi_n(z)\,\mathrm{d}z=N_n\delta_{mn}, \qquad m,n\geq0 \tag{2.42}$$

which extends the definition of k_n to include $n=0$ where $k_0=-\mathrm{i}k$ and

$$N_n=\frac{1}{2}\left(1+\frac{\sin2k_nh}{2k_nh}\right)\sec^2k_nh. \tag{2.43}$$

Note that in the case $n=0$ this becomes

$$N_0=\frac{1}{2}\left(1+\frac{\sinh2kh}{2kh}\right)\mathrm{sech}^2kh. \tag{2.44}$$

In writing (2.40) we have also satisfied the condition

$$\left.\frac{\partial\phi}{\partial x}\right|_{x=0} = \begin{cases} U(z), & a < z < b, \\ 0, & \{0 < z < a\} \cup \{b < z < h\} \end{cases} \tag{2.45}$$

provided

$$\mathrm{i}khN_0(1-R) = \int_a^b U(z)\psi_0(z)\,\mathrm{d}z. \tag{2.46}$$

All that remains is to match the pressure across $x = 0$, $a < z < b$ (noting that $r = z$ on $\theta = 0$) which, by (2.4), is proportional to ϕ and so from (2.39) and (2.40) we have

$$\frac{\pi}{2}zU(z) - K^{-1}(1 - \mathrm{i}/\tilde{\Lambda}(z))U(z) + (\mathcal{K}U)(z) = -(1+R)\psi_0(z), \qquad a < z < b \tag{2.47}$$

where

$$(\mathcal{K}U)(z) \equiv \int_a^b U(z')\kappa(z,z')\,\mathrm{d}z' \tag{2.48}$$

is a real, positive, symmetric integral operator with a kernel defined by

$$\kappa(z,z') = \sum_{r=1}^{\infty} \frac{\psi_r(z)\psi_r(z')}{N_n k_r h}. \tag{2.49}$$

Letting $u(z)$ satisfy

$$\left[\frac{\pi}{2}z - K^{-1}(1 - \mathrm{i}/\tilde{\Lambda}(z))\right] u(z) + (\mathcal{K}u)(z) = \psi_0(z), \qquad a < z < b \tag{2.50}$$

implies that $U(z) = -(1+R)u(z)$ satisfies (2.47). Substituting this relation into (2.46) gives

$$\mathrm{i}khN_0(1-R) = -(1+R)\mathcal{A}, \qquad \text{where} \quad \mathcal{A} = \int_a^b u(z)\psi_0(z)\,\mathrm{d}z. \tag{2.51}$$

In other words, the reflection coefficient may be determined by

$$R = -\frac{\mathcal{A} + \mathrm{i}khN_0}{\mathcal{A} - \mathrm{i}khN_0}. \tag{2.52}$$

We remark that when $\tilde{\Lambda}(z) \to \infty$, equivalent to switching off the power take-off, the integral equation (2.50) becomes real and so the solution $u(z)$ and, hence $\mathcal{A}$, is real. Then $|R| = 1$ implying no energy is absorbed by the device, as must be the case. The limit $\tilde{\Lambda}(z) \to 0$ is equivalent to replacing the power take off with a rigid lid with no compression, the integral equation furnishes $U(z) = 0$ and $|R| = 1$. If just $\tilde{\lambda}_1 = 0$ but $\tilde{\lambda}_2 \neq 0$ then the air turbine is shut off but the air compressibility allows a non-zero flow in the duct. In this case the integral equation is real once again and so $|R| = 1$.

3. Efficiency

Under the inviscid assumption, the mean power, W, absorbed at the OWC is calculated in two different ways. In the first method we equate W to the flux of energy crossing a vertical boundary far from the device. That is

$$W = \lim_{X\to-\infty} \frac{\omega}{2\pi} \int_0^{2\pi/\omega} \int_0^h \Phi_x(X,z,t)(P(X,z,t) - P_a)\,\mathrm{d}z\,\mathrm{d}t. \tag{3.1}$$

In frequency-domain variables

$$W = \lim_{X\to-\infty} \frac{1}{2}\Re\left\{-\frac{\mathrm{i}\rho g^2|A|^2}{\omega}\int_0^h \phi_x(X,z)\overline{\phi(X,z)}\,\mathrm{d}z\right\} = W_{inc}(1-|R|^2) \tag{3.2}$$

after use of (2.14), where the overbar denotes complex conjugate and

$$W_{inc} = \frac{1}{2}\rho g|A|^2 c_g \tag{3.3}$$

is the incident wave energy in terms of the group velocity defined by

$$c_g = \frac{d\omega}{dk} = \frac{g}{\omega}khN_0 \tag{3.4}$$

where N_0 is defined by (2.44). We are interested in the efficiency of power capture $E \in [0,1]$ defined by $E = E_{ff}$ where

$$E_{ff} = \frac{W}{W_{inc}} = 1-|R|^2 \tag{3.5}$$

(the subscript ff is used to indicate this is a calculation made in the far-field). A second method of calculating mean power comes from measuring the mean rate of working of the flux against the pressure across the turbines. According to this definition in terms of the N discrete channels

$$W = \frac{\omega}{2\pi}\int_0^{2\pi/\omega}\sum_{j=1}^{N}\int_{r_{j-1}}^{r_j}\zeta_t(x,t)(P(x,0,t)-P_a)\,\mathrm{d}x\,\mathrm{d}t. \tag{3.6}$$

Invoking homogenisation replaces discrete variables by continuous variables so that

$$W = \frac{1}{2}\frac{\rho g^2|A|^2}{\omega}\Im\left\{-\int_a^b \phi_z(x,0)\overline{\phi(x,0)}\,\mathrm{d}x\right\}. \tag{3.7}$$

Using (3.4), (3.5) gives the efficiency as $E = E_{nf}$ (nf indicates this is a near-field calculation) where

$$E_{nf} = \frac{1}{khN_0}\Im\left\{\int_a^b \frac{1}{r}\frac{\partial\phi}{\partial\theta}(r,\pi/2)\overline{\phi(r,\pi/2)}\,\mathrm{d}r\right\}. \tag{3.8}$$

Inserting the definition (2.39) gives

$$E_{nf} = \frac{1}{khN_0}\Im\left\{\int_a^b \frac{\mathrm{i}}{K\tilde{\Lambda}(r)}|U(r)|^2\,\mathrm{d}r\right\} = \frac{|1+R|^2}{KkhN_0}\Im\left\{\mathrm{i}\int_a^b \frac{|u(z)|^2}{\tilde{\Lambda}(z)}\,\mathrm{d}z\right\} \tag{3.9}$$

after using the relation $U(r) = -(1+R)u(z)$. This simplifies in the case that $\tilde{\Lambda}$ is constant. We see that $\tilde{\lambda}_1$ controls the power take off and the efficiency tends to zero when $\tilde{\lambda}_1 \to \infty$. Note that if $\tilde{\lambda}_2 = 0$ then $E_{nf} \to 0$ as $\tilde{\lambda}_1 \to 0$ since $u(z) \to 0$ also in this case.

4. Numerical approximation

In order to solve the integral equation (2.50) we use a Galerkin method in which the solution is approximated by the $(2M+1)$-term expansion

$$u(z) \approx \sum_{m=-M}^{M} c_m u_m(z) \tag{4.1}$$

where c_m are coefficients to be determined and

$$u_m(z) = \mathrm{e}^{\mathrm{i}m\pi(2z-b-a)/(b-a)} \tag{4.2}$$

are the complex Fourier series basis for the interval $z \in (a, b)$ satisfying

$$\int_a^b u_m(z)\overline{u_q(z)}\,\mathrm{d}z = (b-a)\delta_{qm}. \tag{4.3}$$

Galerkin's method applied to solutions of integral equations involves substituting (4.3) into (2.50) before multiplying by $\overline{u_q(z)}$ for $q = -M, \ldots, M$ and integrating over $a < z < b$. This results in the linear system of equations

$$\sum_{m=-M}^{M} c_m \mathcal{K}_{qm} = \overline{F_{q0}}, \qquad q = -M, \ldots, M \tag{4.4}$$

defining c_m where

$$\mathcal{K}_{qm} = \frac{\pi}{2}T_{qm} - K^{-1}(b-a)\delta_{qm} + \mathrm{i}K^{-1}S_{qm} + \sum_{r=1}^{\infty}\frac{F_{mr}\overline{F_{qr}}}{N_r k_r h} \tag{4.5}$$

and we have written

$$F_{mr} = \int_a^b u_m(z)\psi_r(z)\,\mathrm{d}z \tag{4.6}$$

with

$$S_{qm} = \int_a^b \frac{u_m(z)\overline{u_q(z)}}{\tilde{\Lambda}(z)}\,\mathrm{d}z \qquad \text{and} \qquad T_{qm} = \int_a^b z u_m(z)\overline{u_q(z)}\,\mathrm{d}z. \tag{4.7}$$

Explicit expressions for F_{mr} and T_{qm} are given in Appendix A. In the simplest case that $\tilde{\Lambda}$ is constant, $S_{qm} = (b-a)\delta_{qm}/\tilde{\Lambda}$.

We now use (4.1) in (2.51) to get

$$\mathcal{A} \approx \sum_{m=-M}^{M} c_m F_{m0} \tag{4.8}$$

allowing us to approximate E_{ff} from (3.5) once R is calculated using (2.52).

The alternative calculation of efficiency uses (4.1) in (3.9) to get

$$E_{nf} \approx \frac{4khN_0}{K|\mathcal{A} - \mathrm{i}khN_0|^2}\Im\left\{\mathrm{i}\sum_{n=-M}^{M}\sum_{m=-M}^{M} c_n\overline{c_m}S_{mn}\right\}. \tag{4.9}$$

In the case that $\tilde{\lambda}_1$ and $\tilde{\lambda}_2$ are both constant we have, on account of (4.3),

$$E_{nf} \approx \frac{4khN_0(b-a)^{3/2}}{K^{1/2}|\mathcal{A} - \mathrm{i}khN_0|^2}\cdot\frac{\tilde{\lambda}_1}{\tilde{\lambda}_1^2 + K(b-a)\tilde{\lambda}_2^2}\sum_{n=-M}^{M}|c_n|^2. \tag{4.10}$$

In the work of Parry-Barnard (2025) (not repeated here as it is too much of a diversion from our main goal) it is shown that approximations, made by implementing Galerkin's method, to the solution of the integral equations imply the equivalence of E_{nf} and E_{ff} described previously. Numerical computations bear this out with only small differences due to rounding errors between computed values of E_{nf} and E_{ff}. This is true for any parameters used including the truncation parameter, M. Thus, the two methods are useful

for validating the numerical method, but cannot be used as a means of assessing the accuracy of the numerical results.

5. Viscous losses in the duct

Since the OWC design supposes a cascade of annular baffles separate the curved duct into narrow channels within which the fluid is subjected to resonant excitation, one might therefore be concerned about the role natural dissipative effects have on the device efficiency. Thus, we consider here a simple extension to the previous formulation of the problem which includes the damping due to viscous wall effects. In a full-scale design we reasonably envisage channels within the duct to be large enough that the plug-flow assumption holds across the bulk of each channel ($\Delta \gg \sqrt{\nu/2\omega}$ where ν is the kinematic viscosity). Then the wall stress, per unit length, due to boundary-layer shear associated with the no-slip condition on the walls of the channel is easily calculated (from the solution to the well-known Stokes problem since wall curvature is negligble under the boundary-layer scaling) to be

$$\sigma_{R\theta}|_{R=0,1} = -\mathrm{i}\sqrt{\frac{\nu}{\omega}}\mathrm{e}^{-\mathrm{i}\pi/4}U(r) \tag{5.1}$$

(noting that we have applied the appropriate variable scalings stated in §2 to the stress and to U). Therefore, its integrated effect along the length of each channel, from both walls, can be written

$$-\mathrm{i}\pi r\sqrt{\frac{\nu}{\omega}}\mathrm{e}^{-\mathrm{i}\pi/4}U(r) = \Delta p_{vis}(r) \tag{5.2}$$

which has been related to the jump in pressure needed to overcome viscous damping (Δ is the channel width). This pressure drop needs to be added to the solution in the duct and means that continuity of pressure across $x = 0$ is no longer equivalent to matching ϕ from both sides resulting in (2.47), but requires matching ϕ from $x < 0$ with $\phi - p_{vis}$ from $x > 0$. Thus, instead of (2.47) we have

$$\left[\frac{\pi}{2}z + \frac{\pi z\tilde{\Gamma}\mathrm{e}^{\mathrm{i}\pi/4}}{(K(b-a))^{1/4}} - \frac{(1-\mathrm{i}/\tilde{\Lambda}(z))}{K}\right]U(z) + (\mathcal{K}U)(z) = -(1+R)\psi_0(z), \tag{5.3}$$

for $a < z < b$ where we have written

$$\tilde{\Gamma} = \frac{\nu^{1/2}N}{(b-a)^{3/4}g^{1/4}}, \tag{5.4}$$

a dimensionless constant, independent of frequency, which determines the effect of the viscosity on the OWC design. As expected, $\tilde{\Gamma}$ increases linearly with the number of channels, N.

The impact of the modification (5.3) to (2.47) is easy to follow and eventually the first term $(\pi/2)T_{qm}$ in (4.5) needs to be replaced by

$$\frac{\pi}{2}\left(1 + \frac{2\tilde{\Gamma}\mathrm{e}^{\mathrm{i}\pi/4}}{(K(b-a))^{1/4}}\right)T_{qm} \tag{5.5}$$

in the numerical method.

The two calculations of efficiency made under inviscid assumptions are now no longer equal and E_{nf} is used to calculate the efficiency of power conversion by the device. The larger value of E_{ff} includes losses due to viscous damping. The work of Parry-Barnard (2025) shows how the two formally equate via the integral equation (5.3) by calculating

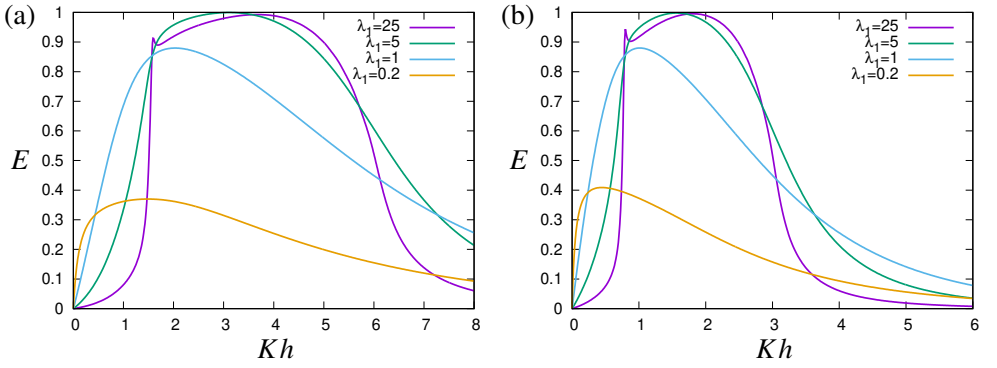

Figure 2. Variation of efficiency with Kh for two designs: (a) with $a/h = 0.1$, $b/h = 0.4$; and (b) $a/h = 0.2$, $b/h = 0.8$. In both cases $\tilde{\lambda}_2 = 0$ and $\tilde{\lambda}_1$ is varied.

the rate of viscous dissipation due to the boundary layers in the channels but the lengthy details are omitted from this paper. The two different calculations of E are useful since $E_{ff} - E_{nf}$ indicates the percentage of incident wave power lost to viscous wall effects.

6. Results

6.1. *Resonance*

The condition for resonance in a narrow curved channel of length l, intersecting the free surface at right angles, is easily shown to be approximated by

$$\omega^2 l/g = 1. \tag{6.1}$$

This is because the mass (per unit length) of fluid in the channel of width Δ is $\rho\Delta l$ and the hydrostatic restoring force due to an internal free surface elevation ζ is $-\rho g\Delta\zeta$. Balancing these two terms under time-harmonic motion of angular frequency ω results in (6.1). This argument ignores wave radiation and local flow conditions at the submerged opening and a more refined calculation for narrow vertical ducts in two and three dimensions is presented in Evans (1978).

The lengths of the channels in the configuration shown in Fig. 1 range from $a\pi/2$ to $b\pi/2$ and so the spectrum of resonance of the array of channels in the duct is given by

$$\frac{2h}{\pi b} < Kh < \frac{2h}{\pi a}. \tag{6.2}$$

In many of the examples below we set $a/h = 0.1$ and $b/h = 0.4$ and then (6.2) gives $1.6 < Kh < 6.36$. This device is designed to be resonant for incident wavelengths between roughly one and four times the water depth.

In Fig. 2(a) we show the computed efficiency E (either E_{ff} or E_{nf}) for this device design over the extended range $0 < Kh < 8$ for a particular choice of $\tilde{\lambda}_1 = 5$ and setting $\tilde{\lambda}_2 = 0$. Alongside in Fig. 2(b), we show computed efficiency for different design parameters, $a/h = 0.2$ and $b/h = 0.8$, where the predicated range of resonance is $0.8 < Kh < 3.18$. Since b/a are the same in both cases, Figs. 2(a) and (b) highlight the effect of fluid depth. The plots indicate that high efficiency is sustained across most of the range of resonance, only tailing off towards the ends.

M	$E\ (Kh = 1)$	$E\ (Kh = 2)$
1	0.3254	0.9821
2	0.3292	0.9533
4	0.3319	0.9588
8	0.3335	0.9577
16	0.3343	0.9575
32	0.3348	0.9574
64	0.3350	0.9573

Table 1. Computed values of efficiency, $E = E_{ff} = E_{nf}$, for increasing truncation parameter, M, for $Kh = 1$ and $Kh = 2$ with $a/h = 0.1$, $b/h = 0.4$, $\tilde{\lambda}_1 = 5$ and $\tilde{\lambda}_2 = 0$.

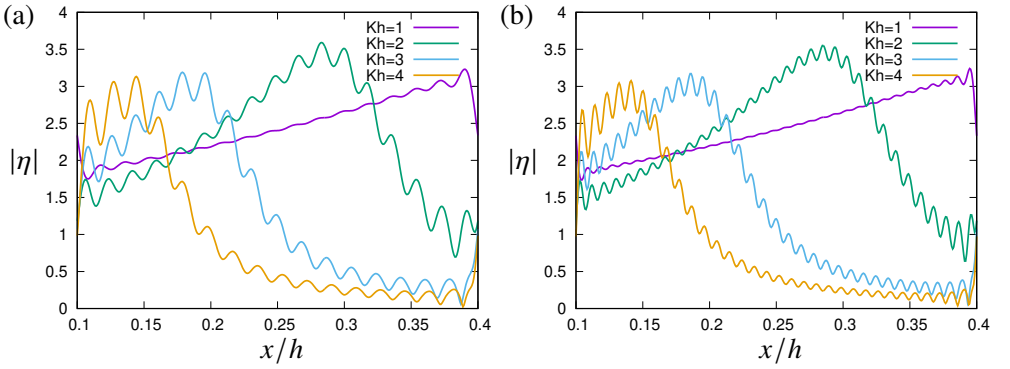

Figure 3. Plots of the modulus of $\eta(x)$ against $x/h \in (0.1, 0.4)$ for $a/h = 0.1$, $b/h = 0.4$, $\tilde{\lambda}_1 = 5$, $\tilde{\lambda}_2 = 0$ for three different values of Kh. Plots (a) and (b) are for $M = 16$ and $M = 32$.

6.2. *Convergence of the numerical method*

There are two parameters which control the accuracy of the numerical solutions. The first is the number of terms included in the infinite series defining $\mathcal{K}_{qm}$ in (4.5). For this, it has been found that 100 terms is sufficient for the numerical accuracy required to compute the efficiency to three decimal places. The second is the value of M which controls the number of terms taken in the expansion of the approximate solution in (4.1). In Tab. 1 we present a convergence example for a typical set of results in the middle of the resonant range of frequencies. We are reminded that the two values of $E = E_{ff}$ and $E = E_{nf}$ are numerically identical (apart from small rounding errors) and cannot be used to indicate accuracy of the method.

In Fig. 3(a,b) we show the computed value of $|\eta|$, the modulus of the internal free surface amplitude non-dimensionalised by the incident wave height, as a function of $z \in (a, b)$. For this, we use the relation $|\eta| = |1 + R||u(z)|/K$. Results are shown for truncation sizes of $M = 16$ and $M = 32$ for a fixed geometry and constant power control. The oscillations in the curves are explained by Gibbs phenomenon, but nevertheless demonstrate the convergence of approximations with increasing M. In each figure curves represent different values of Kh to show how resonance is excited in positions along the duct dependent on frequency. For the device parameters chosen, $Kh = 1$ is outside the resonant spectrum. Fig. 3(a,b) show that, for the parameters chosen, device resonance corresponds to less than a doubling of the standing wave amplitudes that would occur if waves were reflected by a wall without the device in place.

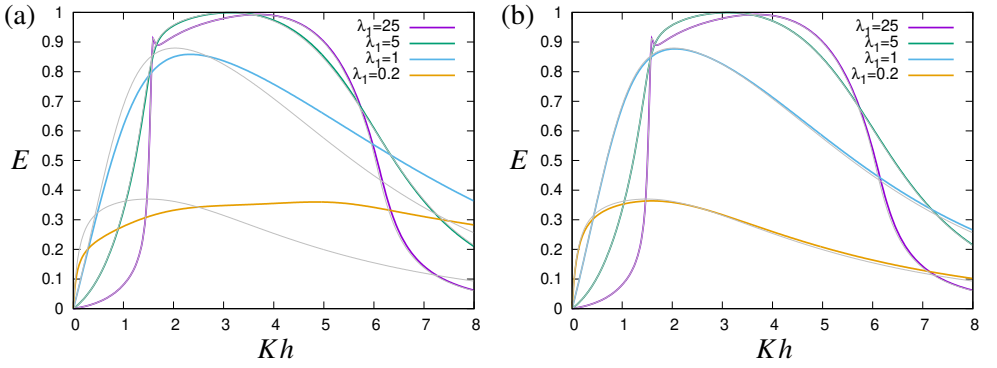

Figure 4. Variation of efficiency with Kh for $a/h = 0.1$, $b/h = 0.4$ In (a) $\tilde{\lambda}_2 = 0.333$ and in (b) $\tilde{\lambda}_2 = 0.033$; $\tilde{\lambda}_1$ is varied. The grey curves shadow the values computed in Fig. 2.

6.3. *The role of compressibility of air*

The effect of compressibility in (4.9) is controlled by the size of the ratio of the imaginary and real parts of $\tilde{\Lambda}$, or

$$(Kh(b/h - a/h))^{1/2}(\rho g H/\rho_a c_a^2)/\tilde{\lambda}_1 \approx 0.07H\sqrt{Kh(b/h - a/h)}/\tilde{\lambda}_1 \qquad (6.3)$$

(in SI units). For a full-scale installation we imagine H to be roughly 4−5m and $(b/h-a/h)$ to be roughly $0.3 - 0.5$ whilst it seems reasonable to assume that $Kh \lesssim 6$ is a range of practical interest (implying wavelengths no shorter than the water is deep). Then the maximum size of (6.3) is roughly $0.5/\tilde{\lambda}_1$. So compressibility can become a significant factor if $\tilde{\lambda}_1$ is roughly one or less and for larger values of Kh. In terms of producing the optimal power output, it has been found that we should choose $\tilde{\lambda}_1 \approx 5$, not only for results shown in Fig. 2 but also for other configurations tested. Then the size of the term in (6.3) never exceeds 0.1 and we expect the effect of drag on the efficiency to be proportionately small. These observations are bourne out in the results shown in Fig. 4(a).

In experiments one might imagine $H = 0.4 - 0.5$m and then the size of the term in (6.3) is an order of magnitude smaller than in the full-scale setting meaning its effect is negligible as shown in Fig. 4(b).

6.4. *The role of viscosity*

The size of $\tilde{\Gamma}$ defined by (5.4) in a full-scale installation is estimated to be of the order of 10^{-3} based, say, on 6 channels within a duct of the size $b - a = 3$m. This is much smaller than the other $O(1)$ terms in (5.4). Even with many more channels, the influence of viscosity at full scale is going to be negligible. In experiments, we might imagine $b - a = 0.3$m in which case $\tilde{\Gamma}$ is more like 10^{-2} and likely to still have only a small effect on results. Sample results are shown in Fig. 5(a).

6.5. *Non-constant control parameters*

We consider the effect of introducing spatial control of the damping by letting $\tilde{\lambda}_1(z) = \alpha e^{-\beta z}$ where $\alpha > 0$ and $\beta \neq 0$ are constants. For $\beta > 0$ the damping is weaker for the longer channels and vice versa whilst $\beta = 0$ corresponds to constant damping considered previously. Setting $\tilde{\lambda}_2 = 0$ allows us to explicitly calculate the terms required in the numerical scheme (see Appendix A). Fig. 5(b) shows the results of fixing $\alpha = 5$ and varying $\tilde{\beta} = \beta/(b - a)$ between -2 and 2. Other combinations of α and $\tilde{\beta}$ have been considered but, as shown in Fig. 5(b), it seems that spatial control of damping does not result in significant improvements in the efficiency.

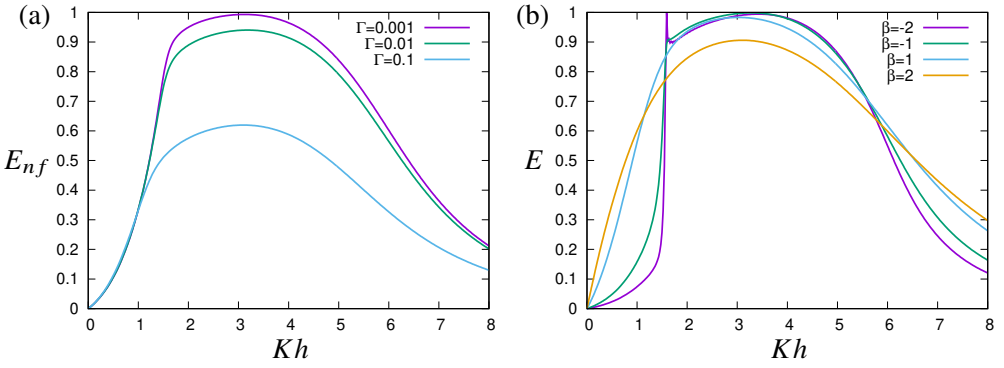

Figure 5. Variation of device efficiency with Kh for $a/h = 0.1$, $b/h = 0.4$. In (a) $\tilde{\lambda}_1 = 5$, $\tilde{\lambda}_2 = 0$ and different values of $\tilde{\Gamma}$; in (b) spatially-varying power control: $\alpha = 5$ and different values of $\tilde{\beta}$.

6.6. *Comparison with a simple single chamber OWC*

In Fig. 6 we have plotted a comparison of the performance, in terms of efficiency, of the current multi-channel (or multi-chamber) OWC design against the single-chamber OWC design of Evans & Porter (1995) for two cases. In the first case, the multi-chamber OWC parameters are $a = 0.25h$ and $b = 0.75h$ and this is compared to the Evans & Porter (1995) results with a barrier submergence of $0.25h$ and chamber width $0.75h$. In the second example, we have chosen $a = 0.1h$, $b = 0.99h$ and results are compared to Evans & Porter (1995) with a barrier submergence of $0.1h$ and chamber width h. In each case, air compressibility and viscous effects have been neglected and the value of the damping parameters for each curve produced have been chosen to 'optimise' the efficiency profile. Thus, we can see that the multi-chamber OWC design does no better than a single chamber design if immersion of the duct opening is too large. For a smaller immersion of the duct opening, the multi-chamber OWC outperforms the single chamber OWC by a significant degree.

7. Conclusions

We have considered a two-dimensional model of an novel OWC concept which has been designed to exploit resonance over a broad range of frequencies. A simple mathematical model has been formulated by approximating the complexity of the multi-channel duct using homogenisation. The general conclusion drawn from the various numerical experiments considered here is that the optimal configuration of an OWC, resulting in a high bandwidth, can be achieved by applying constant power control across the array of channels. It has been found that the effects of compressibility and viscosity may be neglected when applied to a full-scale installation, although these effects might influence test-scale experiments.

From an engineering perspective a multi-chamber design is more complicated than a single chamber OWC. However, the technology already exists for smaller Wells turbine (the Mutriku plant uses generators rated at 19kW) than were used for the larger installations at the LIMPET and PICO pilot plants. The nature of the ocean energy density spectrum means that loads will be distributed across multiple generators in the array. As the device is designed to be fixed, tidal variation is an issue although the broadbanded response of the device allows it function across a range of conditions. Moreover, the multi-channel design allows for a system of louvres which shut different channels on and off to optimise

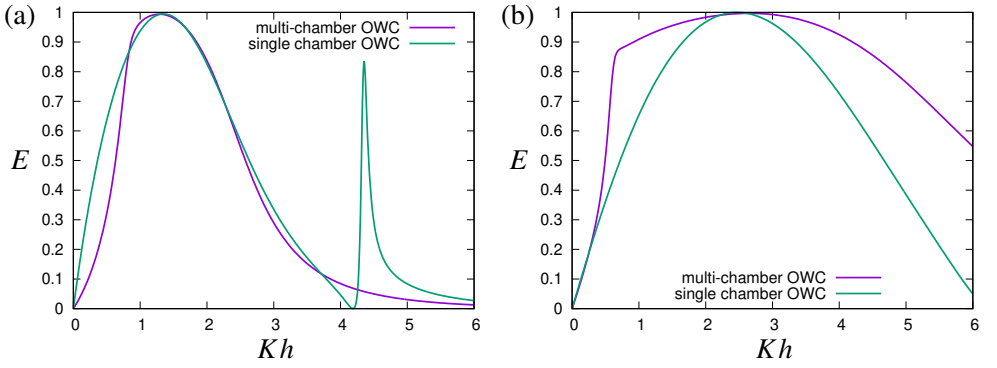

Figure 6. Comparision of efficiency with Kh for the current multi-chamber design and the single chamber OWC of Evans & Porter (1995) in the cases that the front wall immersion is: (a) $0.25h$; and (b) $0.1h$.

performance in different sea conditions as well as being used for a complete shutdown of the device in storms.

Extensions to the current work might involve solving the problem of distinct channels within the duct exactly, without homogenisation. This might require the use of boundary element methods even for the two-dimensional problem because semi-analytic methods are not easy to apply to such geometries. It is possible to consider a three-dimensional version of this problem for a segmented OWC of finite width in an infintely-long wall using a combination of the methods described here and Fourier transforms. One would need to make a convincing case for adding extra complexity.

Funding This research received no specific grant from any funding agency, commercial or not-for-profit sectors.

Declaration of Interests The authors report no conflict of interest.

Author ORCIDs R. Porter, https://orcid.org/0000-0003-2669-0188, S. Parry-Barnard, https://orcid.org/0009-0006-5464-8293

Appendix A

Below are the explicit definitions of the terms required in the numerical scheme. We define $c = \frac{1}{2}(a+b)$ and $d = \frac{1}{2}(b-a)$. In the case that $r \neq 0$ we have

$$F_{mr} = \frac{2d(-1)^m \sin k_r d}{((k_r d)^2 - (m\pi)^2)\cos k_r h}\left[k_r d \cos k_r(h-c) + \mathrm{i}m\pi \sin k_r(h-c)\right] \tag{A 1}$$

and when $r = 0$ this is

$$F_{m0} = \frac{2d(-1)^m \sinh kd}{((kd)^2 + (m\pi)^2)\cosh kh}\left[kd \cosh k(h-c) + \mathrm{i}m\pi \sinh k(h-c)\right]. \tag{A 2}$$

Next we find that

$$T_{qq} = 2cd, \qquad \text{and} \qquad T_{qm} = \frac{2d\mathrm{i}(-1)^{q+m}}{(q-m)\pi}, \quad (q \neq m). \tag{A 3}$$

When $\tilde{\lambda}_1(z) = \alpha \mathrm{e}^{-\beta z}$, $\tilde{\lambda}_2 = 0$ we have

$$S_{qm} = \frac{2d\mathrm{e}^{\beta c}}{\alpha}(-1)^{m+q}\frac{\sinh \beta d}{\mathrm{i}\pi(m-q)+\beta d}. \tag{A 4}$$

References

Boake, C.B., Whittaker, T.J.T., Folley, M., & Hamish E. 2002 Overview And Initial Operational Experience of the LIMPET Wave Energy Plant. *The 12th Int. Offshore and Polar Engng Conf.*, Kitakyushu, Japan.

Evans, D.V. 1978 The Oscillating Water Column Wave Energy Device. *IMA J. Appl. Math.*, **22**(4), pp.423–433.
Evans, D.V. 1981 Power from the waves. *Ann. Rev. Fluid Mech.*, **13**, pp.157–187.
Evans, D.V. 1982 Wave-power absorption by systems of oscillating surface pressure distributions. *J. Fluid Mech.*, **114**, pp.481–499.
Evans, D.V. and Porter, R. 1995 Hydrodynamic characteristics of an oscillating water column device. *Appl. Ocean Res.*, **17**(3), pp.155–164.
Falcão, A.F. de O. and Sarmento, A.J.N.A. 1980 Wave generation by a periodic surface pressure and its application in wave-energy extraction. *15th Int. Congress Theor. Appl. Mech.*, Toronto.
Falcão, A.F. de O. and Henriques, J.C.C. 2016 Oscillating-water-column wave energy converters and air turbines: A review. *Renewable Energy*, **85**, pp.1391–1424.
Falcão, A.F. de O., Sarmento, A.J.N.A., Gato, L.M.C. and Brito-Melo, A. 2020 The Pico OWC wave power plant: Its lifetime from conception to closure 1986–2018. *Appl. Ocean Res.*, **98**, 102104.
Falnes, J. 1993 Research and development in Ocean-wave energy in Norway. *Int. Symp. on Ocean Energy Development* Muroran, Hokkaido, Japan.
Gayathri, R., Chang J.-Y., Tsai, C.-C. and Hsu, T.-W. 2024 Wave energy conversion through oscillating water columns: A review. *J. Marine Sci. Engng.*, **12**(2), p. 342.
Heath, T.V. 2012 A review of oscillating water columns. *Phil. Trans. Roy. Soc. A.*, **370**(1959), pp.235–245.
Hu, Y., Cheng Y., Dai, S., Yuan, Z., Inececik, A. 2025 Broadband wave conversion by a "Pan Flute"-type multi-oscillating-water-column (M-OWC) breakwater system. *Energy Conversion and Management* **333**, 119820.
Liang, H., Porter, R. & Zheng, S. 2024 Wave scattering by plate array metacylinders of arbitrary cross-section. *J. Fluid Mech.* **1001**:A6.
Linton, C.M. and McIver. P. 2001 *Handbook of Mathematical Techniques for Wave/Structure Interactions.* Chapman and Hall/CRC.
Lopez-Mendia, J., Aristondo, A., Ricci, P., Lekube, J., Ceballos, S., and Robles, E. 2025 Improving the power production of Mutriku wave power plant throughout tuning the actual generator and damping valve limits. *Ocean Engng.*, **315**, 119917.
Martin-Rivas, H. and Mei, C.C. 2009 Wave power extraction from an oscillating water column along a straight coast. *Ocean Engng.*, **36**(6-7), pp.426–433.
Masuda, Y. 1985 An experience of wave power generator though tests and improvement. In *Hydrodynamics of Ocean Wave Energy Utilization Symposium.* D.V. Evans, A.F. de O. Falcão (eds.), Lisbon, Portugal.
Parry-Barnard, S. 2025 *The Theoretical Efficiency of a Novel Design of Oscillating Water Column Device.* M.Sc. thesis, University of Bristol, UK.
Porter, R. 2025 Hydrodynamic characteristics of an oscillating water column device – revisited. `https://people.maths.bris.ac.uk/~marp/abstracts/eandp95.pdf`.
Sarmento, A.J.N.A. and Falcão, A.F. de O. 1985 Wave generation by an oscillating surface-pressure and its application in wave-energy extraction. *J. Fluid Mech.*, **150**, pp.467–485.
Smith, C.M. 1983 *Some problems in linear water waves.* Ph.D. thesis, University of Bristol, UK.
Whittaker, T.J.T., Leitch, J.G., Long, A.E. & Murray, M.A. 1985 The Q.U.B. Axisymmetric and Multi-Resonant Wave Energy Convertors. *J. Energy Resour. Tech.*, **107**(1), pp.74–80.
Wilks B., Montiel F., Wakes S. 2022 Rainbow reflection and broadband energy absorption of water waves by graded arrays of vertical barriers. *J. of Fluid Mech.*, **941**:A26.
Zheng, S., Antonini, A., Zhang, Y., Greaves, D., Miles, J. & Iglesias, G. 2019 Wave power extraction from multiple oscillating water columns along a straight coast. *J. Fluid Mech.*, **878**, pp.445–480.